## Title

Redox-Triggered Release of Moxifloxacin from Mesoporous Silica Nanoparticles Functionalized with Disulfide Snap-Tops Enhances Efficacy Against Pneumonic Tularemia in Mice.



## Journal

Small (Weinheim an der Bergstrasse, Germany), 12(27)

## ISSN

1613-6810

## Authors

Lee, Bai-Yu
Li, Zilu
Clemens, Daniel L
et al.

## Publication Date

2016-07-01

## DOI

10.1002/smll.201600892

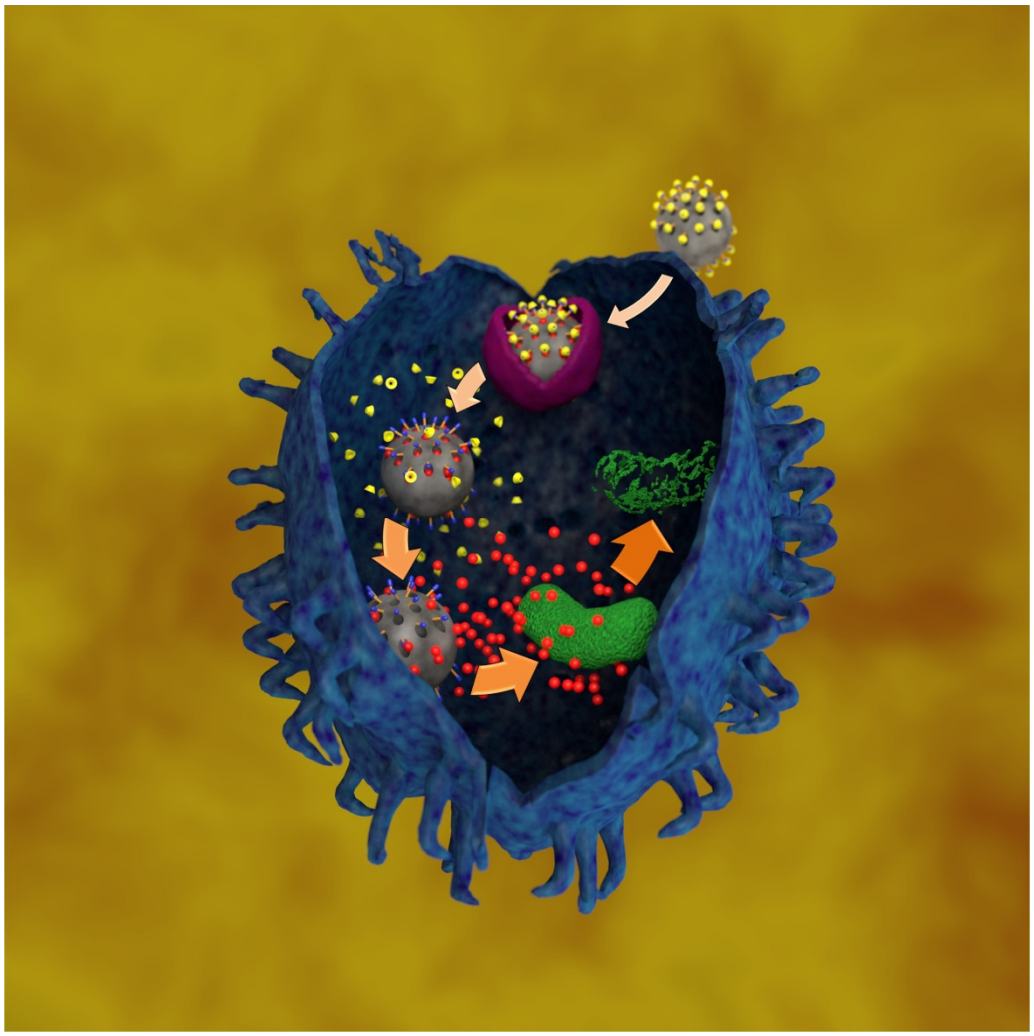

**TOC.** Depiction of the drug trapping and intracellular release mechanism of MSN-SS-MXF. MSN-SS-MXF are mesoporous silica nanoparticles functionalized with disulfide snap-tops that carry a large quantity of the broad spectrum antibiotic moxifloxacin within its pores. The snap-top has a bulky β-cyclodextrin cap that blocks the pores until it is detached by reducing agents, such as occur naturally in the intracellular environment, releasing the cargo. MSN-SS-MXF naturally targets macrophages, releases the antibiotic in response to the intracellular redox potential, and kills intracellular bacterial pathogens, such as *Francisella tularensis*, *in vitro* and *in vivo*.

# Redox-triggered Release of Moxifloxacin from Mesoporous Silica Nanoparticles Functionalized with Disulfide Snap-Tops Enhances Efficacy Against Pneumonic Tularemia in Mice

**Bai-Yu Lee, Zilu Li, Daniel L. Clemens, Barbara Jane Dillon, Angela A. Hwang, Jeffrey I. Zink*, and Marcus A. Horwitz***

Dr. B.-Y. Lee, Prof. D. L. Clemens, B. J. Dillon, Prof. M. A. Horwitz
Division of Infectious Diseases
Department of Medicine
University of California
Los Angeles, CHS 37-121, 10833 Le Conte Ave., CA 90095-1688, USA
E-mail: mhorwitz@mednet.ucla.edu

Dr. Zilu Li, Dr. A. A. Hwang, Prof. J. I. Zink
Department of Chemistry and Biochemistry
University of California
Los Angeles, 3013 Young Dr. East
CA 90095-1569, USA
E-mail: jiz@chem.ucla.edu

Prof. J. I. Zink
California NanoSystems Institute
University of California
Los Angeles, CA 90095-8352, USA

Dr. Zilu Li
Department of Materials Science and Engineering
University of California
Los Angeles, CA 90095, USA

*Address correspondence to Marcus A. Horwitz, mhorwitz@mednet.ucla.edu or Jeffrey Zink, zink@ucla.edu

**Conflict of interest:** The authors have declared that no conflict of interest exists.

## Abstract

Effective and rapid treatment of tularemia is needed to reduce morbidity and mortality of this potentially fatal infectious disease. The etiologic agent, *Francisella tularensis*, is a facultative intracellular bacterial pathogen which infects and multiplies to high numbers in macrophages. Nanotherapeutics are particularly promising for treatment of infectious diseases caused by intracellular pathogens, whose primary host cells are macrophages, because nanoparticles preferentially target and are avidly internalized by macrophages. We have developed a mesoporous silica nanoparticle (MSN) functionalized with disulfide snap-tops that has high drug loading and selectively releases drug intracellularly in response to the redox potential. These nanoparticles, when loaded with Hoechst fluorescent dye, release their cargo exclusively intracellularly and stain the nuclei of macrophages. The MSNs loaded with moxifloxacin kill *F. tularensis* in macrophages in a dose-dependent fashion. In a mouse model of lethal pneumonic tularemia, MSNs loaded with moxifloxacin prevent weight loss, illness, and death, markedly reduce the burden of *F. tularensis* in the lung, liver and spleen, and are significantly more efficacious than an equivalent amount of free drug. This study provides an important proof-of-principle for the potential therapeutic use of a novel nanoparticle drug delivery platform for the treatment of infectious diseases.

**Keywords:** intracellular delivery, redox potential, *Francisella tularensis*, disulfide snap-top, multifunctional mesoporous silica nanoparticle

## Introduction

*Francisella tularensis* is a highly infectious bacterium that causes a life threatening disease, tularemia. Inhalation of as few as 25 bacteria is sufficient to cause severe illness.[1] Its extremely high infectivity, ease of dissemination by the air borne route, and capacity to cause severe disease motivated its development as a biological weapon by Japan during the second World War[2] and by both the U.S. and the former Soviet Union during the cold war.[3] Although effective antibiotics for treatment of tularemia are available, intensive care is frequently required, relapse and complications are frequent, and the infection can be fatal even with appropriate treatment. Concern over its potential for use as a biological weapon has led to its federal classification as a Tier 1 Select Agent. It has been estimated that deliberate dispersal of *F. tularensis* over a large city would overwhelm health care facilities and result in thousands of deaths.[4] Development of more effective treatment for tularemia has the potential to reduce the number of patients requiring intensive care and to reduce the duration that such care is required. Because *F. tularensis* causes disease primarily by replicating intracellularly within host macrophages,[5] a delivery strategy that targets macrophages and delivers high concentrations of antibiotic to the macrophages has the potential to provide more effective treatment.

After systemic administration, nanoparticles are avidly taken up by macrophages of the mononuclear phagocyte system in the lung, liver, and spleen.[6-8] Because these are the cells infected by *F. tularensis*, a nanoparticle delivery system has the potential to deliver high concentrations of antibiotic to the site of infection while minimizing systemic exposure. Nanoparticles also have several other advantages over free drug, including shielding the drug from metabolism and excretion and providing more favorable pharmacokinetics. While several different nanoparticle delivery platforms have been studied for antibiotic delivery, including

liposomes, solid lipid particles, poly-L-lactide (PLGA), and biological materials such as gelatin, chitosan, and alginates,[9, 10] mesoporous silica nanoparticles (MSNs) offer several important advantages, including structural and chemical stability, uniformity, inherent lack of toxicity, capacity to encapsulate exceptionally high concentrations of different types of cargo, and versatility in incorporating rational design features, including stimulus responsive drug release systems.[11-17] In this work, we have developed a stimulus-responsive MSN platform for treatment of tularemia that delivers the antibiotic moxifloxacin (MXF) intracellularly in response to the intracellular redox potential.

Living cells have more reducing power than extracellular medium or plasma because of numerous redox couples that are kept primarily in the reduced state by metabolic processes such as glycolysis, mitochondrial electron transport, and the pentose phosphate pathway. These redox couples include NADH/NAD; NADPH/NADP; thioredoxin/oxidized-thioredoxin, cysteine/cystine, and glutathione (GSH)/GSSG, with the latter redox couple being quantitatively the most abundant inside cells, with cytosolic GSH concentrations in the 1 -10 mM range.[18] Extracellularly, in culture medium and in plasma, the cysteine/cystine redox couple is quantitatively the most important. Disulfide snap-top MSNs release cargo selectively intracellularly because the redox potential is much lower in the intracellular than in the extracellular environment.[19, 20] On the basis of the intracellular glutathione/glutathione disulfide ratio, the redox potential is estimated to range from -250 mV in rapidly dividing cells to -200 mV in differentiating cells to -160 mV in cells undergoing apoptosis.[21] Different compartments within the cell also maintain different ambient potentials; for example, based on the thioredoxin redox poise, the cytoplasm, nucleus, and mitochondria exhibit redox potentials of -280, -300, and -340 mV, respectively.[20] On the other hand, the GSH/GSSG redox couple in plasma has a redox

potential of -140 mV[22] and the much more abundant cysteine-cystine is even more oxidized, with a redox potential of -80 mV.[23] A similar situation is replicated in cell culture model systems, as human cell lines regulate the redox state of the cysteine-cystine couple in their culture medium to approximately -80 mV.[24] Prior to addition to cultured cells, cysteine-free RPMI-1640 has a relatively high redox potential of -37 mV and RPMI supplemented with 0.45 mM cysteine has a redox potential of -182 mV.

Disulfide snap-top MSNs utilizing cyclodextrin as the cap have been reported previously.[19, 25, 27-29] The original version involved a rotaxane where α-cyclodextrin (α-CD) threaded on a stalk was held in place by a bulky stopper on the end of the disulfide-containing stalk.[19] Subsequent versions used direct covalent bonding of β-cyclodextrin (β-CD) to a stalk[27] and noncovalent bonding of β-CD to adamantine at the end of stalks of different lengths.[25, 28, 29] In this paper the functionality of the snap-top with the shortest (propyl group) stalk is discussed. Although streptomycin and aminoglycosides are historically considered the treatment of choice for tularemia, they cross membranes poorly, have relatively high minimum inhibitory levels against *F. tularensis,* have side effects of ototoxicity and nephrotoxicity, and are difficult to administer. Doxycycline or ciprofloxacin are recommended for post-exposure treatment in a mass casualty setting.[3] In contrast to aminoglycosides, fluoroquinolones cross membranes readily and have much lower minimal inhibitory concentrations against *F. tularensis*. Ciprofloxacin has been used successfully both in animal models of tularemia[30] and in the treatment of clinical tularemia infections.[31] In a mouse model of pneumonic tularemia comparing ciprofloxacin, gatifloxacin, and MXF, while all three fluorquinolones showed efficacy during the treatment phase, both MXF and gatifloxacin were superior to ciprofloxacin in preventing relapse, indicating greater efficacy in eradicating the *F. tularensis*.[32] Because of its

potent antimicrobial activity against *F. tularensis* as well as potent activity against many other important intracellular human pathogens, including *Mycobacterium tuberculosis*,[33] *Listeria monocytogenes*,[34] *Mycoplasma*, *Chlamydia*, *Shigella*, and *Salmonella,* we developed our redox-responsive disulfide snap-top MSNs (MSN-SS-MXF) for delivery of MXF.

In this study, we demonstrate that our MSN-SS-MXF delivery platform releases its antibiotic cargo intracellularly in macrophages, is effective in killing *F. tularensis* in infected macrophages in a cell culture model, and is a much more effective treatment than an equivalent amount of free drug in a mouse model of pneumonic tularemia.

## Results

### Synthesis of Disulfide Snap-top MSNs

To utilize MSNs to deliver MXF into macrophages and release the drug intracellularly in a controlled fashion, we developed a disulfide snap-top attached to the surface of the MSN so as to trap drug inside mesopores. The synthesis procedure is illustrated in Figure 1. A silane stalk (3-mercaptopropyl) trimethoxysilane was attached on the surface of MSN first and then 1-adamantanethiol reacted with the silane linker in the presence of the oxidant thiocyanogen to form a disulfide bond (Figure S1, Supporting Information). The modified MSNs preserve mesoporous structures after all surface modification and surfactant template extraction procedures (Figure S2), and the particles exhibit a mean diameter of 90 nm by DLS measurement in $H_2O$. Disulfide modified MSN was then mixed with MXF PBS solution for 24 h, followed by adding β-CD as the capping molecule which formed a stable complex with the adamantyl group. In reducing environments (e.g. after addition of glutathione or after uptake by macrophages), the disulfide bond is cleaved and cargo is released. It's possible that in the intracellular environment competitive binding for the β-CD may also occur and contribute to cargo release. The strong binding affinity between the adamantyl group and β-CD ensure that cargo is trapped inside the pores and prevents premature leakage before reaching target cells.

An alternative method reported by others for constructing redox-sensitive valves is to attach an admantyl group covalently to the particle surface .[27] In that case, one more chemical reaction is required, after drug loading, to form the amide bond. This extra synthetic step requires that the drug-loaded particles (without capping) be suspended in solution in order to attach the caps. During this step, drugs can diffuse out of the pores and catalyst molecules can diffuse into the pores and contaminate the cargo.

The snap-top used in this paper contains a short (propyl group) linker in order to hold the β-CD caps close to the pore openings and inhibit leakage. The chemicals used in the synthesis procedure, illustrated in Figure 1, are both commercially available.

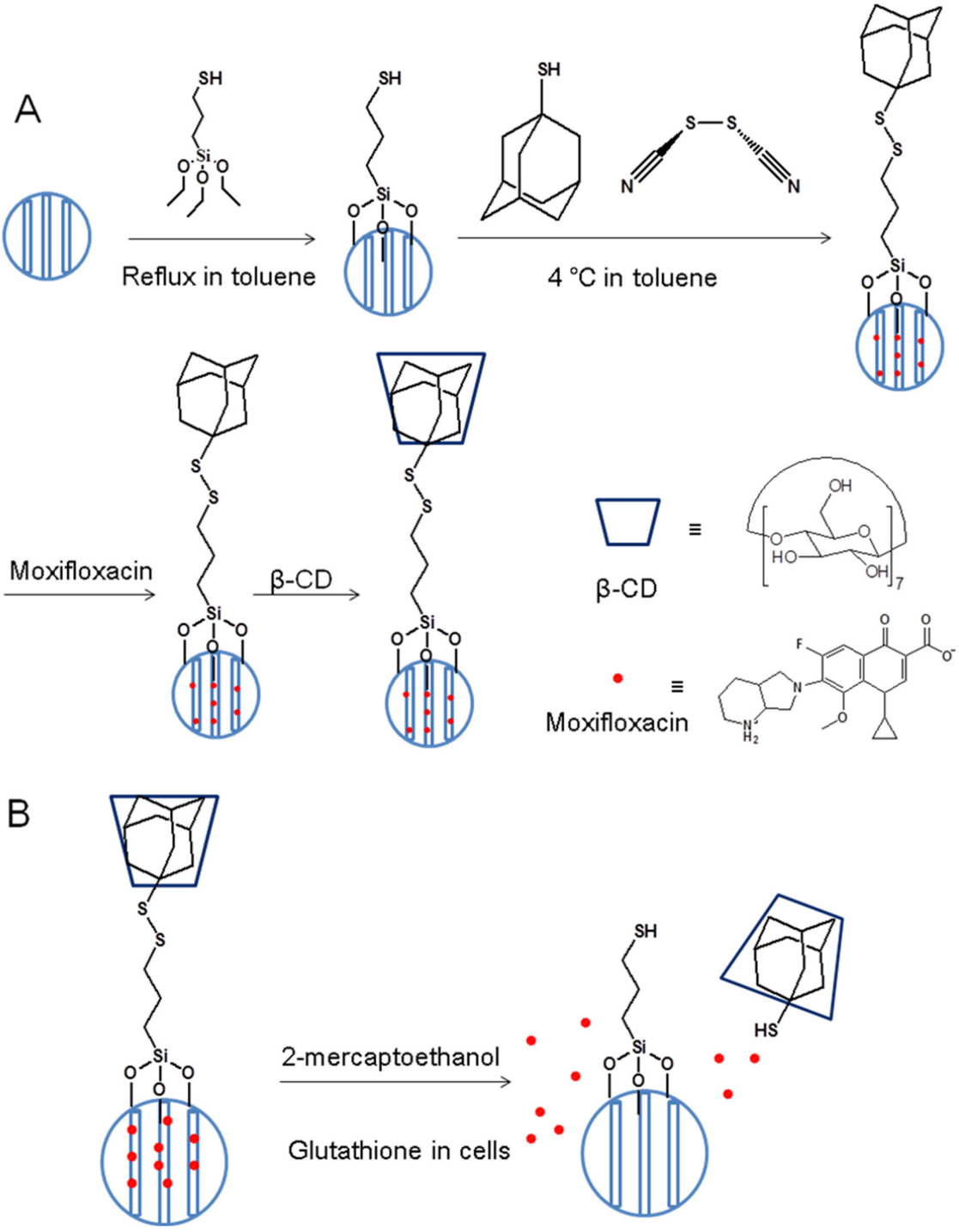

**Figure 1.** Disulfide snap-top system synthesis and release mechanism. A) First, a silane stalk (3-mercaptopropyl) trimethoxysilane is attached to the surface of the MSN. Subsequently, 1-adamantanethiol is reacted with the silane linker in the presence of the oxidant thiocyanogen to form a disulfide bond. Disulfide modified MSNs are then loaded with MXF, followed by the addition of β-cyclodextrin (β-CD) as the capping molecule. B) The disulfide bond on the thread is cleaved by the reducing agent, 2-mercaptoethanol in the laboratory or glutathione inside cells, removing the bulky β-CD cap and releasing MXF from the pores of the nanoparticle.

MXF is a fourth generation fluoroquinolone active against both Gram-positive and Gram-negative bacteria. It has a UV-Vis maximum absorption peak at 288 nm in PBS allowing spectroscopic measurement of its concentration. We measured the absorbance of MXF in solution before and after loading the nanoparticles and used the difference in concentration to calculate the amount of MXF taken up by the particles (including inside pore channels and on external surfaces). The mass of MXF taken up by particles divided by the mass of MSNs is defined as “uptake capacity” (expressed in wt%). After washing mechanized MSN with PBS sufficiently to remove MXF from the outer surface, the nanoparticles were dispersed in deionized water or PBS and then an excess amount of 2-mercaptoethanol or glutathione was added to cleave the disulfide bond and release the drug (Figure 2). The mass of released MXF divided by the mass of the particle is defined as “release capacity” (expressed in wt%). Moreover, the flat baseline before adding the reducing agent indicates that no premature release occurs and that there is strong binding between the adamantyl group and β-CD.

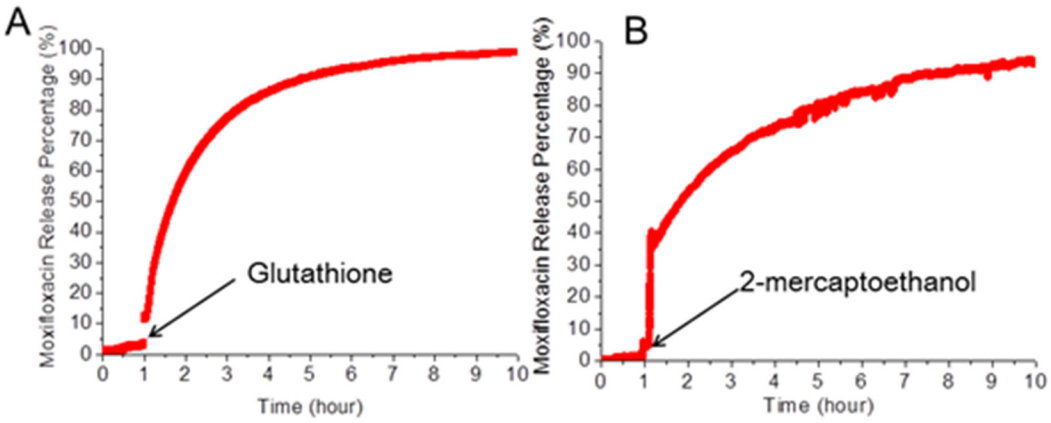


**Figure 2.** MSN-SS-MXF is released by MXF in DI water when A) glutathione or B) 2-mercaptoethanol is added and cleaves the disulfide bond.

**Optimization of Uptake and Release Capacity**

Release capacity of a nanoparticle delivery system is an important factor that impacts *in vivo* efficacy, as a higher release capacity allows a greater amount of drug to be delivered to target cells with the same number of MSNs. We exploited charge interactions between the cargo molecules and the MSN inner pores to achieve a high uptake and release capacity. MXF has two ionizable groups with p*K*a's of 6.3 and 9.3, and the extent to which the drug is positively charged, neutral, or negatively charged is pH-dependent. Hence, the pH of the loading solution markedly impacts uptake capacity. In PBS buffer with pH 7.4, 87.8% of MXF molecules are zwitterionic species, 7.3% molecules are positively charged, and 4.8% are negatively charged. We modified the MSNs with either amine groups or phosphonate groups to make both the inner pore and outer particle surface positively or negatively charged, respectively. Positively charged cargo interacts electrostatically with negatively charged pores, thereby increasing the uptake capacity; however, strong electrostatic interaction between cargo molecules and pore channels

may also slow the rate of cargo release.[35] On the other hand, positively charged pores electrostatically repulse the positively charged cargo molecules, thereby decreasing the uptake capacity but facilitating and increasing the rate of cargo release.

Before attaching snap-top caps, we measured the uptake capacity of MSNs with different pore charges and found that with positively charged mesopores the uptake capacity was near zero, indicating that it is too difficult for MXF molecules with a positive net charge to diffuse into positively charged MSN channels. Use of negatively charged pores dramatically increased the uptake capacity to 30 wt% and the release capacity to 3 wt% (10 mM MXF in a volume of 1 mL PBS) (Table S1A, Supporting Information). Other experiments showed that a further increase in negative charge on pores does not improve uptake and release capacity. Pore modification was achieved by co-condensation of two silanes, in which diethylphosphatoethyltriethoxysilane (DEPETS) was mixed with tetraethyl orthosilicate (TEOS) and then added to heated base solution in a dropwise fashion. Different amounts of DEPETS (10 μL, 25 μL and 35 μL) were mixed with TEOS (60 μL) to make more negatively charged pores, and these nanoparticles showed similar release capacity of ~2-3 wt% under the same loading conditions (Table S1B, Supporting Information). This result suggested that the amount of phosphonate groups inside the pores is saturated and hence the attraction of positively charged MXF molecules is maximized.

We also tested loading MSN-SS in solutions of different pH because in acidic solutions, most of MXF molecules are positively charged and interact with negatively charged inner pores, resulting in a higher uptake capacity. However, lowering pH may also render phosphonate groups on inner pores partially protonated and thus less negatively charged, resulting in a lower uptake capacity. Experiments showed that loading with pH 3 MXF solution (1 mL 10 mM)

resulted in 9.6 wt% uptake capacity, which is much lower than the 22.2 wt% uptake capacity obtained when loading with pH 7.4 MXF solution (1 mL 10 mM). The enhanced uptake capacity at pH 7.4 is due to more negatively charged mesopores at this pH (Table S1C, Supporting Information).

Moreover, we compared the uptake capacity of MSNs (10 mg) with 10 μmol disulfide stalk surface coverage with that of MSNs with 20 μmol surface coverage. We hypothesized that the higher surface coverage would cap more MXF molecules inside the pores. However, we obtained uptake capacities of 22.2 wt% and 19.7 wt% with surface coverage of 10 μmol and 20 μmol, respectively, which indicated that higher surface coverage with the silane stalks may increase the surface hydrophobicity of MSNs and lower the uptake of the hydrophilic drug MXF (Table S1D, Supporting Information). Therefore, 10 μmol disulfide stalk surface coverage provided a satisfactory balance between hydrophobicity and capping MXF within pores so as to achieve high uptake.

To obtain a higher uptake and release capacity, we loaded the same amount of MSN-SS with a more concentrated MXF PBS solution (40 mM MXF in a volume of 1mL PBS vs. 10 mM MXF in a volume of 1mL PBS). This yielded an uptake and release capacity of 135 wt% and 51 wt%, respectively, the highest release capacity yet obtained (Table S1E, Supporting Information). This result indicates that the osmotic gradient of the loading system is an additional major factor impacting uptake and release capacity of MSN-SS-MXF. Considering a) the MSN's inner pores charges; b) the MSN's concentration of phosphonate groups; c) the MSN's disulfide stalk surface coverage; d) the loading concentration of MXF; and e) the loading pH, we found the optimal conditions to be negatively charged phosphonated MSNs (10 μL

DEPETS / 10 mg) with disulfide stalk surface coverage of 10 μmol loaded with 1mL 40 mM MXF in PBS solution (pH 7.4).

**Measurement of MSN-SS-MXF Release Capacity**

We used a *F. novicida* bioassay (Figure S3, Supporting Information) to determine the maximum amount of MXF released from particles. With this assay we measured the amount of drug released from MSN-SS-MXF in PBS or DMSO with and without 2-mercaptoethanol by determining the inhibition of *F. novicida* growth in broth cultures. We measured a release capacity for MSN-SS-MXF of 12 wt% in PBS and a total of 18 wt% after addition of reductant. When MSN-SS-MXF was dispersed in DMSO with 2-mercaptoethanol, the bioassay measurement showed a release capacity of 51 wt%. The higher release capacity in DMSO with 2-mercaptoethanol indicates that not all MXF molecules were released from mesopores in PBS. In comparison, the highest release capacity obtained from using the pH-sensitive nanovalve was around 8 wt%.[11]

**Disulfide Snap-Top MSNs Release Cargo at Physiological GSH Concentrations**

Quantitatively, GSH is the major reducing agent in cells, with intracellular concentrations of approximately 10 mM in healthy cells.[36, 37] To determine whether the disulfide snap-tops operate at physiological concentrations of GSH, we loaded disulfide snap-top MSNs with Hoechst 33342, a membrane permeant probe for double-stranded DNA, and incubated them with 0 – 16 mM GSH in PBS for 18 h at room temperature. The nanoparticles were pelleted by centrifugation and the supernates were diluted 20-fold with RPMI culture medium and added to monolayers of human macrophage-like THP-1 cells. The cells were incubated for 3 h at 37 ºC, stained with WGA-AF633 to label the plasma membranes, fixed, and the Hoechst staining of the

nuclei measured by fluorescence microscopy. We observed increasing Hoechst staining of the cell nuclei with increasing GSH concentrations in the physiological 1 – 10 mM range, confirming that the snap-top valves function at physiological intracellular concentrations of GSH (Figure 3).

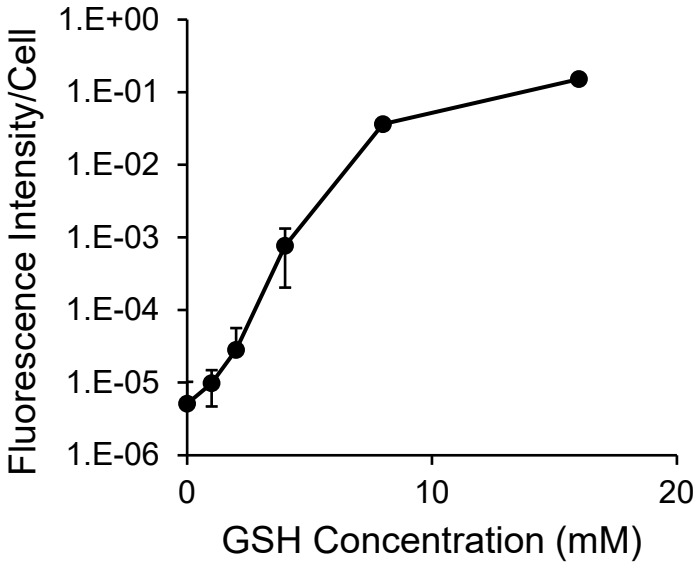


**Figure 3.** Hoechst dye release from MSN-SS snap-top by physiological concentrations of GSH in RPMI culture medium. Snap-top nanoparticles (1 mg/mL) loaded with the membrane permeant DNA stain Hoechst 33342 were incubated with various concentrations of GSH ranging from 0 – 16 mM, as indicated, overnight at room temperature. The nanoparticles were pelleted by centrifugation and the supernate was diluted 20-fold with RPMI culture medium and added to THP-1 cells. Cells were incubated for 3 h at 37 ºC, stained with WGA-AlexaFluor 633, fixed, and examined by fluorescence microscopy with fixed exposure and gain settings. Data are relative fluorescence intensity of the Hoechst staining per cell as quantitated using CellProfiler.

**Release of Cargo in Response to Intracellular Environment**

To investigate whether the disulfide snap-top valves work properly inside of cells, we used the MSNs to deliver Hoechst 33342. We added Hoechst loaded disulfide snap-top MSNs and eluate prepared from the MSNs in PBS (non-reducing condition) to THP-1 macrophages and incubated at 37 °C for 18 h. We observed that nuclei of THP-1 cells were stained after incubation with Hoechst 33342 loaded disulfide snap-top MSNs, but not after incubation with the PBS eluate of the MSNs (Figure 4). These results provide strong evidence that the disulfide snap-top valves open to release cargo in the intracellular reducing environment.

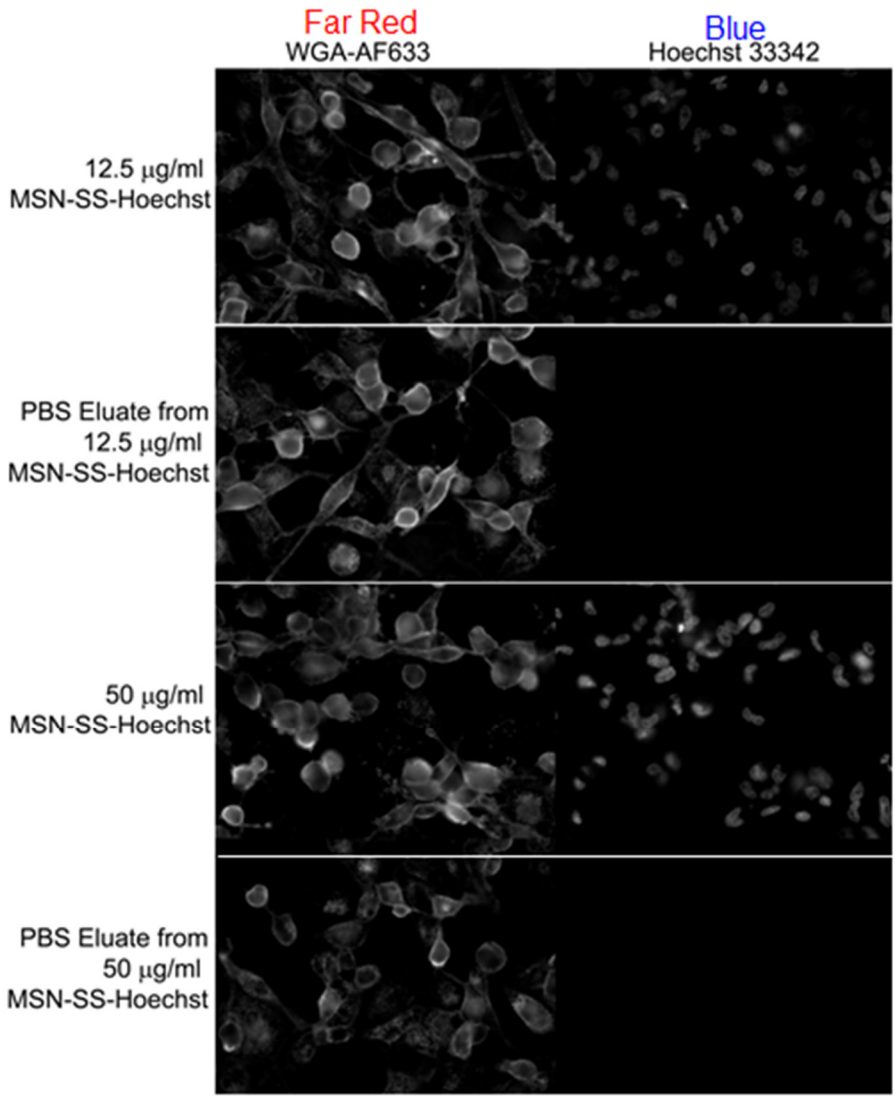

**Figure 4.** MSN-SS-Hoechst but not their PBS eluates stain the nuclei of THP-1 cells. THP-1 macrophages were incubated with snap-top MSNs loaded with the membrane permeant DNA stain Heochst 33342 (MSN-SS-Hoechst) or the PBS elulate from MSN-SS-Hoechst for 18 h, fixed with 4% paraformaldehyde, and incubated with Alexa Fluor 633-conjugated wheat germ agglutanin (WGA) to stain the plasma membrane of the cells. Images were acquired with a Nikon Optishot microscope equipped with SPOT RKT camera using SPOT software and fixed exposure and gain settings.

**Disulfide Snap-top MSNs are Taken Up by Human Macrophages and Kill Intracellular *F. tularensis***

We assessed the efficacy of the disulfide snap-top MSNs loaded with MXF (MSN-SS-MXF) in a macrophage model of *F. tularensis* infection. We infected THP-1 macrophages with *F. tularensis* Live Vaccine Strain (LVS) and treated the infected macrophages with serial two-fold increasing concentrations of MSN-SS-MXF or free MXF. The infected macrophages that were not treated were lysed at 3 h and 1 day post infection to monitor bacterial growth. All infected macrophages that were treated were lysed at 1 day post infection to determine the impact of each treatment on bacterial viability in macrophages by enumerating colony forming units (CFU).

While with no treatment the bacteria grew 2.5 logs in one day, treatment with MSN-SS-MXF (6.25 – 400 ng/mL) or MXF (1 – 64 ng/mL) reduced bacterial CFU in macrophages in a dose-dependent manner (Figure 5A and C). The amount of releasable drug loaded on the disulfide snap-top MSNs was determined by the level of bacterial killing using supernatants prepared from the MSNs under a) aqueous PBS non-reducing condition; b) aqueous PBS with

reducing agent 2-mercaptoethanol; and c) organic DMSO with reducing agent 2-mercaptoethanol. By comparing the amount of killing by supernatants prepared from MSN-SS-MXF with the amount of killing by free drug (Figure 5C), we determined the releasable drug loading under aqueous non-reducing, aqueous reducing, and organic reducing conditions to be 4.9 wt%, 9.9 wt% and 27.4 wt%, respectively. The higher percentage of drug release under organic reducing conditions indicates that MXF is strongly adsorbed to MSN through hydrophobic interactions. Hence, in addition to a reducing condition, a hydrophobic environment, such as DMSO or an intracellular environment is required for efficient release of MXF from the disulfide snap-top MSN carrier.

Based on the drug release capacity of 27.4 wt%, the impact of MXF delivered by various doses of the MSN-SS-MXF in killing of *F. tularensis* LVS was compared with that of free drug using a median-effect plot.[38] As shown in Figure 5D, the median-effect plot of the MSN-SS-MXF is almost superimposable on that of the free drug, indicating that MXF delivered by the disulfide snap-top MSN has an efficacy equal to that of free MXF in the *in vitro* macrophage model of *F. tularensis* LVS infection.

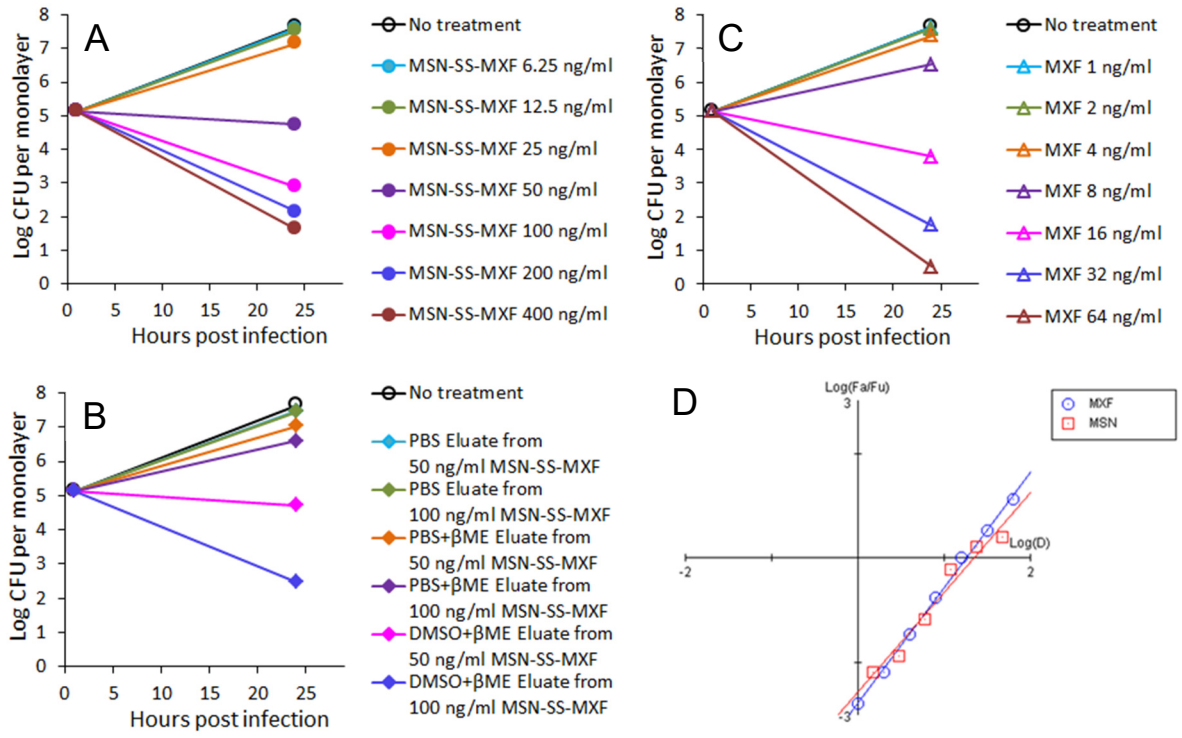


**Figure 5.** MSN-SS-MXF is as effective as MXF in killing *F. tularensis* in human macrophages. PMA-differentiated THP-1 macrophages were infected with *F. tularensis* LVS and treated with various doses of A) MSN-SS-MXF, B) eluates prepared from MSN-SS-MXF incubated in aqueous PBS with and without reducing agent 2-mercaptoethanol (βME) or in DMSO with βME or C) free MXF. Bacterial colony forming units (CFU) in the macrophages with or without treatment were determined at 30 min and 24 h post infection. D) The impact of MSN-SS-MXF and MXF treatment on bacterial viability was compared using median-effect analysis. Median-effect curves generated by CompuSyn for free MXF and an equivalent amount of MXF on the nanoparticle (MSN) were plotted in the same graph. Log(D) is dose of free MXF or MXF equivalent of MSN-SS-MXF in logarithm; Log(Fa/Fu) is the division of the fraction of bacteria killed (Fa) by the fraction of bacteria surviving (Fu) in logarithm.

**MSN-SS-MXF is Much More Efficacious than an Equivalent Amount of Free MXF in a Mouse Model of Pneumonic Tularemia**

We assessed the efficacy of the MSN-SS-MXF in a mouse model of pneumonic tularemia established previously for evaluation of vaccine candidates.[39-41] In the first of two experiments (Experiment 1), mice were infected by the intranasal route (i.n.) with 4000 CFU of *F. tularensis* LVS, a dose equivalent to about 6 times the $LD_{50}$. One day later, the bacterial number in the lung increased by 1.5 logs. Without treatment, the bacteria continued to grow in the lung and disseminate to other organs. At the end of the 6-day infection period, the bacterial number reached approximately $10^7$ in the lung and $10^5$ - $10^6$ in the liver and spleen (Figure 7A and C). One day after infection, mice were treated with 50, 100 or 200 μg of free MXF or 260 μg of the MSN-SS-MXF (loaded with 91 μg free MXF) per dose by tail vein injection every other day for a total of 3 treatment doses. During the course of infection, sham (PBS)-treated control mice suffered significant weight loss, whereas mice treated with free MXF or MSN-SS-MXF maintained their body weights (Figure 6A).

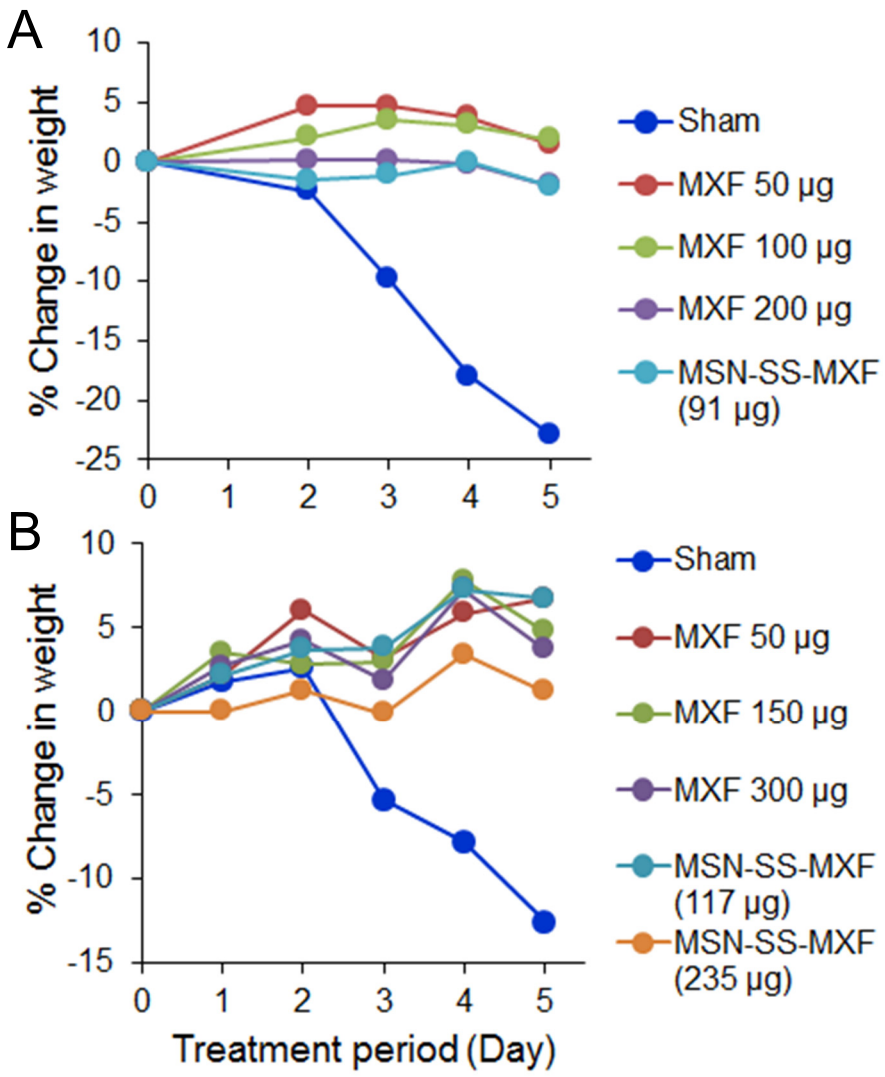


**Figure 6.** Treatment with MSN-SS-MXF prevents weight loss in mice infected with *F. tularensis*. Mice with pneumonic tularemia were weighed daily during the course of treatment. A,B) Data shown are percentage change in weight of mice in two independent experiments. The mice were sham-treated, treated with three different doses of the broad spectrum antibiotic MXF administered as a free drug, or treated with one or two doses of MSN-SS-MXF, as indicated.

Bacterial burden in the lung, liver and spleen was determined on Day 6, one day after the last treatment dose. With 34.9 wt% release capacity measured under organic reducing conditions, the total amount of intracellularly releasable MXF from 260 μg of MSN-SS-MXF per treatment dose was calculated to be 91 μg. Treatment with MSN-SS-MXF reduced the bacterial burden in the lung and spleen by 3.9- and 4.3-logs, respectively; a reduction greater than that achieved by free MXF at the dose of 200 μg (Figure 7C). MSN-SS-MXF treated animals also showed reduced bacterial burden in the liver to a level below that of free MXF at a dose of 100 μg. The differences in bacterial burden reduction in the lung and spleen between treatment with MSN-SS-MXF loaded with 91 μg MXF and treatment with an equivalent amount of free MXF (adjusted mean computed from the logit scale linear dose response curve for three doses of free drug as described in methods) were highly significant with P-values of 0.00001 and 0.00002, respectively; however, in the liver, the difference between treatment with MSN-SS-MXF and an equivalent amount of free MXF did not reach statistical significance. These results demonstrate that treatment with MSN-SS-MXF is more efficacious than treatment with an equivalent amount of free MXF in the lung and spleen with an efficacy ratio (MSN-SS-MXF : free MXF) of ~3-4 : 1 in the lung and spleen, and an efficacy ratio of ~1 : 1 in the liver (Figure S4, left panel, Supporting Information).

In Experiment 2, we assayed the efficacy MSN-SS-MXF using two doses (230 μg and 460 μg) of the MSN [51 wt% release capacity] and three doses (50 μg, 150 μg and 300 μg) of free MXF. Mice were infected by the intranasal route (i.n.) with 2400 CFU of *F. tularensis* LVS, a dose equivalent to about 4 times the $LD_{50}$. Over the course of the *F. tularensis* infection, weight loss in sham control mice was observed after day 3 and declined steadily afterward to the end of the experiment (Figure 6B). In contrast, there was no net weight loss for mice treated with

free MXF or MSN-SS-MXF. This confirms the observation made from the previous experiment that the MSNs are well tolerated by the mice. Organ bacterial burdens were lowered in mice treated with increasing concentrations of MXF administered as free drug. In the lung, mice treated with 50, 150, and 300 μg of MXF reduced bacterial burden from the level in sham-treated animals by 1.3, 2.3, and 2.9 log CFU, respectively. With a 51 wt% release capacity, mice treated with 230 μg and 460 μg MSN-SS-MXF per dose could release 117 μg and 235 μg MXF *in vivo*. The differences in bacterial burden reduction in the lung between mice treated with MSN-SS-MXF loaded with 117 or 235 μg MXF and mice treated with an equivalent amount of free MXF (adjusted mean) were highly significant with a P-value of 0.0001 for MSN-SS-MXF loaded with 117 μg MXF vs. an equivalent amount of free MXF and a P-value of 0.0006 for MSN-SS-MXF loaded with 235 μg vs. an equivalent amount of free MXF. Looked at another way, CFU in the lungs of mice treated with MSN-SS-MXF loaded with 117 μg releasable MXF was 0.75 logs lower than that of mice treated with 300 μg of free MXF, the highest dose of free MXF tested in the experiment (Figure 7B). Thus, MXF delivered by the disulfide snap-top MSN is more efficacious than 3-fold the equivalent amount of free MXF in the lung.

Bacterial burden in the liver and spleen at 5 h and 1 day post-infection were below the limit of detection for the experiment. By day 6, treatment with both doses of MSN-SS-MXF (loaded with 117 and 235 μg MXF) kept bacterial CFU below the level obtained by treatment with 300 μg MXF, the highest dose of free MXF tested in the experiment. In the spleen, the bacterial burdens in mice treated with either dose of MSN-SS-MXF were below the experimental limit of detection. In contrast, *F. tularensis* LVS were detected in the liver as well as in the spleen of mice treated with all three doses of free MXF (Figure 7D). In this second mouse experiment, the difference in reduction of bacterial burden between mice treated with MSN-SS-

MXF loaded with 117 µg MXF and mice treated with an equivalent amount of free MXF (adjusted mean) was statistically significance for both the spleen (P value = 0.00003) and the liver (P value = 0.002). These results demonstrate that MSN-SS-MXF is much more efficacious than an equivalent amount of free MXF in the lung, spleen, and liver with an efficacy ratio (MSN-SS-MXF : free MXF) of ~5 : 1 in the lung, ~3 : 1 in the spleen, and ~3 : 1 in the liver (Figure S4, right panel, Supporting Information).

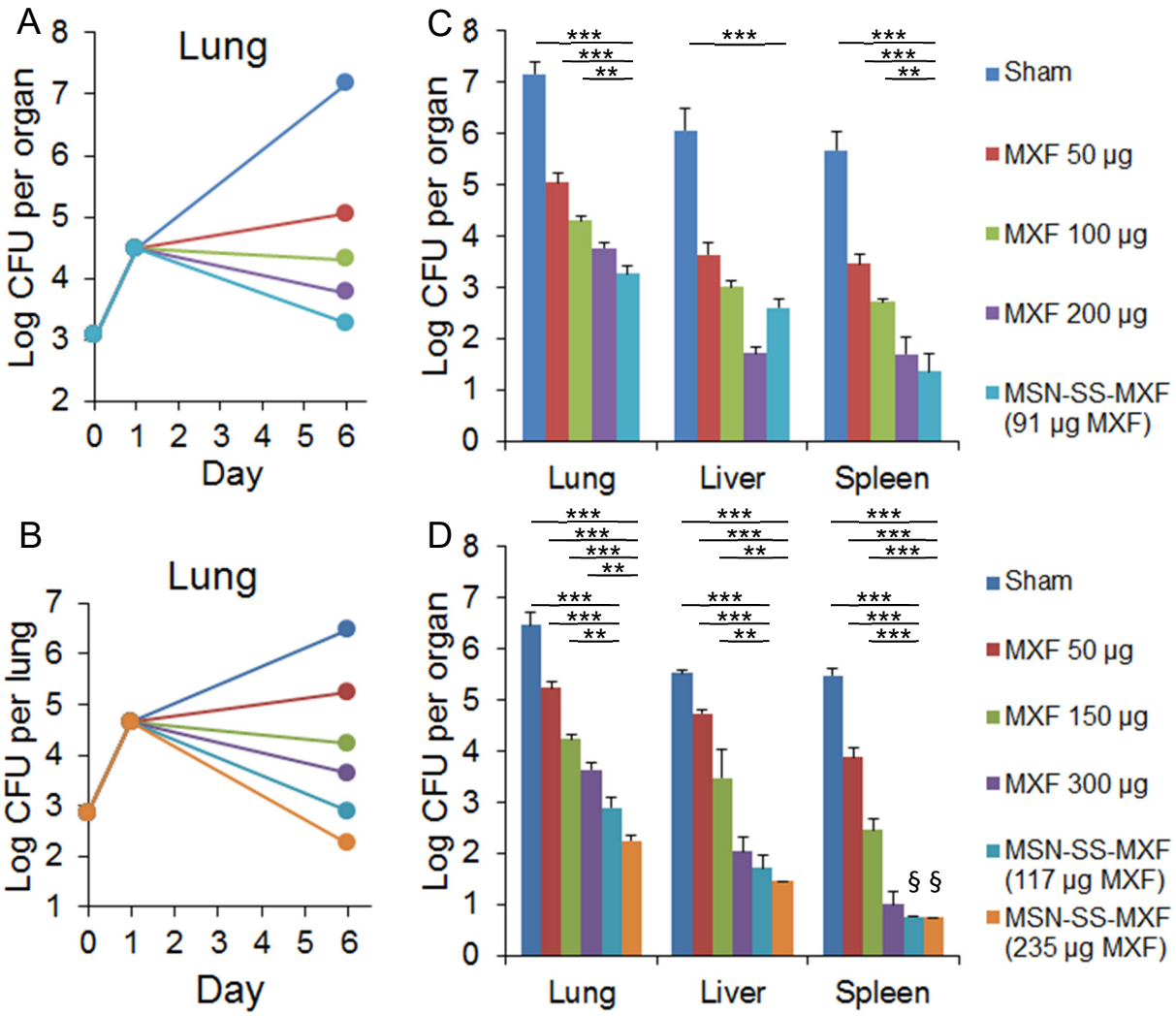


**Figure 7.** *In vivo* efficacy of MSN-SS-MXF in two independent experiments, A,C) Experiment 1 and B,D) Experiment 2. Mice were infected with *F. tularensis* LVS by the intranasal route. A,B)

Bacterial burden in the lung was monitored over the course of infection. One day post-infection, mice were sham-treated (3 mice/group), treated with one of the three doses of free MXF as indicated (3 mice/group), or treated with MXF delivered by the disulfide snap-top MSN (MSN-SS-MXF) by tail vein injection (4 mice/group). C,D) The effect of each treatment on *F. tularensis* burden in lung, liver, and spleen was determined by assaying the bacterial CFU one day after the final treatment. The equivalent amount of free MXF for the MSN-SS-MXF is shown in parenthesis. Statistics were analyzed using one-way ANOVA with Bonferroni post-test correction. $^{**}p < 0.01$, $^{***}p < 0.001$. Error bars represent standard errors. § Bacterial CFU below limit of detection.

We evaluated the biodistribution of the snap-top MSN following tail vein injection 24 h after single or repeated doses in infected mice by inductively coupled plasma optical emission spectrometry (ICP-OES) analysis of the silicon content in the animal organs. The MSNs were euthanized 24 h after a single dose (Figure 8A) or after 3 injections administered every other day over 5 days (Figure 8B). In both cases, the silica of the MSNs is found predominantly in the lung, liver, and spleen, the same three organs that are preferentially targeted by *F. tularensis*. Organs from infected mice that received repeated i.v. injections of PBS were also subjected to ICP-OES analysis. The amount of silica found in these control organs was negligible, indicating a very low background silica level in the organs (Figure 8C).

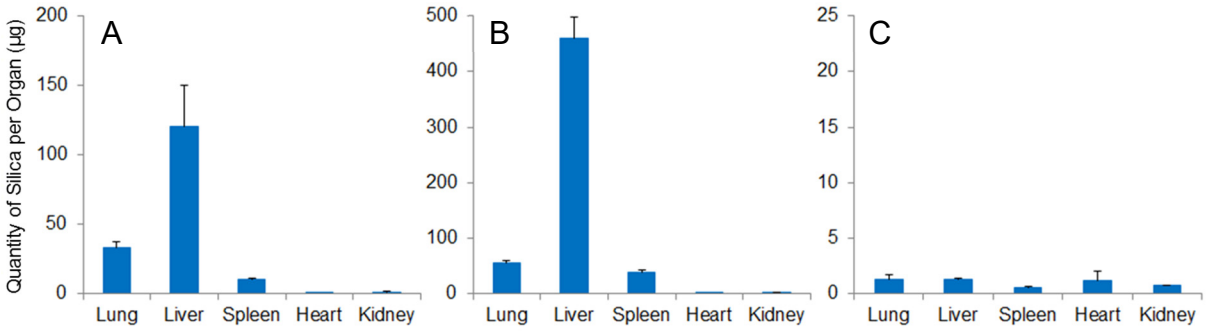


**Figure 8.** Distribution of MSN-SS-MXF in animal organs. Mice were injected via tail vein with A) a single dose or B) three doses of MSN-SS-MXF (460 µg) every other day over 5 days or C) sham-treated with three doses PBS every other day over 5 days and euthanized 24 h after the last injection. Lung, liver, spleen, heart and kidney were assayed for silica by ICP-OES analysis. A similar distribution pattern is observed after A) a single or B) three repeated injections of MSN-SS-MXF, with the majority of the silica found in the liver, lung and spleen. C) Sham-treated mice showed low background levels of silica in their organs; note different scales in the three figures. Data represent means ± standard errors of results from 3 mice per experimental condition with 3 technical repeats per mouse.

## Discussion

Numerous serious human infections, including those caused by *Mycobacterium tuberculosis*, *Salmonella*, *Brucella*, *Legionella pneumophila*, and *F. tularensis*, are caused by microbes that replicate intracellularly in macrophages of the mononuclear phagocyte system. These pathogens exploit the intra-macrophage niche as a source of nutrients and a shelter against host defenses. The macrophage can also pose an obstacle to conventionally administered antibiotics that must cross its plasma membrane and often additional intracellular membranes enclosing the pathogen. Because nanoparticles are preferentially internalized by macrophages of the mononuclear phagocyte system, they are attractive as a drug delivery platform for infections cause by these pathogens. A nanoparticle delivery platform that releases drug exclusively intracellularly has the potential to release high concentrations of drug into infected cells, thus providing for a greater killing efficacy relative to free drug and at the same time limiting systemic exposure to the drug and off-target toxicities. The nanoparticle delivery platform also has the potential to improve the pharmacokinetic profile of the drug by shielding it from excretion and metabolism before it reaches its target cells. Key to the success of such a nanoparticle delivery system is a disulfide snap-top mechanism that releases the drug cargo only after uptake of the nanoparticle into the host cell. Several different mechanisms have been developed to provide for autonomously controlled release of drug cargo from mechanized nanoparticles in response to the intracellular environment, including pH, competitive binding, enzymatic activation, and redox potential.[17, 19, 35, 42-48] Each system has unique chemistry and must be optimized for its drug cargo to achieve maximum loading and controlled release. In the case of the important antibiotic MXF, we have demonstrated that we can achieve very high loading and controlled intracellular release at physiological GSH levels using MSNs functionalized with disulfide snap-tops. Indeed, loading

and release of MXF into MSN-SS-MXF were far superior (release capacity 5-fold greater) to that achieved in a previous study in which we utilized pH-gated MSNs.[11] Consistent with this, the MSN-SS-MXF were more efficacious than the MXF-loaded pH-gated MSNs in treating pneumonic tularemia in mice, as evidenced by higher efficacy ratios vs. free drug in the lung, spleen, and liver.[11] MSNs taken up by macrophages will enter the endosomal-lysosomal pathway, which may have a lower concentration of GSH than the cytosol. In addition, γ-interferon (often elevated in infections) has been shown to lower GSH levels in macrophages.[49] However, lysosomes have a powerful γ-interferon-inducible lysosomal thiol reductase (GILT)[50] capable of cleaving disulfide linkages, including those present in β-CD-based polyrotaxanes therapeutics for lysosomal storage disease.[51]

Modification of the mesopores with phosphonate groups has allowed us to increase the loading and release capacity of our MSNs, and functionalization of the MSNs with a disulfide-cleavable capping system provides for very tight closure of the mesopores under extracellular conditions, preventing premature release of drug cargo, yet allows for ready opening of mesopores and release of mesopore-bound drug cargo in response to the intracellular environment. While redox-responsive disulfide gate mechanisms have been described,[19, 25] they have not previously been tested *in vitro* or *in vivo* for safety or efficacy in the delivery of an antibiotic for treatment of an intracellular pathogen. Ma *et al.* used a similar cap and thread system for delivery of doxorubicin by disulfide snap-top MSNs in a cell culture system and in zebra fish,[29] although we have used a different synthetic route for attaching the adamantane. Most of the previously reported MSN disulfide-snap-tops have used a different chemistry for their redox sensitive gates.[52-62]

We have shown that our disulfide snap-top MSN loaded with MXF is safe and well tolerated *in vitro* and *in vivo*. Importantly, we demonstrated the successful treatment of a serious infectious disease, pneumonic tularemia, using the MSN-SS-MXF. In our cell culture model, the MSN-delivered MXF showed efficacy equivalent to that of free MXF. In contrast, in our *in vivo* mouse model of pneumonic tularemia, the MSN-delivered MXF was three to five times more efficacious than free drug. The difference in efficacy ratios for our *in vitro* vs. *in vivo* models likely reflects the fact that with the *in vitro* model, the macrophages in cell culture wells are exposed to a constant concentration of drug over the course of the experiment whether it is released from the MSNs or administered as free drug. In contrast, in the mouse model of pneumonic tularemia, the efficacy of the MXF administered as free drug is reduced because it is subject to metabolism and excretion and there is no preferential targeting of free drug to tissues or cells that are infected by *F. tularensis*. Hence, the MSN-delivered MXF can achieve higher levels in the infected tissues and host cells than free MXF. Indeed our ICP-OES analysis demonstrated preferential uptake of the MSN by lung, liver, and spleen, which are the main tissues infected by *F. tularensis*. In addition, because MSN-encapsulated drug is shielded from metabolism and excretion, it is likely to have a more favorable Area Under the Curve/Minimal Inhibitory Concentration (AUC/MIC) ratio compared with free drug. The 3- to 5-fold enhanced efficacy of MSN-SS-MXF compared with free drug serves as proof-of-principle that this platform has potential to provide more effective treatment for tularemia as well as other important infections caused by bacteria that multiply intracellularly in macrophages. The average efficacy ratio of MSN-SS-MXF in the lung vs. free moxifloxacin of ~4:1 was superior to that of our previously described pH-gated nanoparticle (MSN-MBI-MXF) which had an average efficacy ratio in the lung of ~3:1 vs. free moxifloxacin. With our current design, the MSNs

passively target infected macrophages, but it is likely that even greater enhancement of therapeutic efficacy can be achieved by surface modifications (e.g. targeting to specific cellular receptors) that further enhance targeting to infected tissues and uptake by macrophages or by use of an aerosol delivery device that delivers the MSNs directly to the lung, as has recently been demonstrated for liposomally encapsulated ciprofloxacin in treatment of tularemia.[63]

## Conclusions

We have developed a redox-responsive disulfide snap-top MSN-drug delivery platform that achieves high uptake and release capacity for the broad spectrum antibiotic MXF by optimizing the MSN inner pore charges, the loading pH, stalk surface coverage density, and the loading concentration of MXF. These MXF-loaded disulfide snap-top MSNs are taken up avidly by *F. tularensis*-infected human macrophages and kill the bacterial pathogen in macrophages *in vitro*. Most importantly, these nanoparticles are much more effective than an equivalent amount of free drug in treating lethal pneumonic tularemia in a mouse model. Our study demonstrates the utility of nanotherapeutics in treating serious and potentially fatal infectious diseases caused by intracellular pathogens.

## Experimental Section

*Materials and Reagents*: Cetyltrimethylammonium bromide (CTAB, 95%), tetraorthoethyl-silicate (TEOS, 98%) 3-(trihydro-xysilyl)propyl methylphosphonate (42% in $H_2O$), 1-adamantanethiol (95%), 2-mercaptoethanol, lead thiocyanate (99.5%), β-cyclodextrin (≥97%), Hoechst 33342 (≥97%), and toluene (99.8%) were purchased from Sigma (St. Louis, MO). (3-mercaptopropyl) trimethoxysilane, N-(2-Aminoethyl)-3-aminopropyltrimethoxysilane (NAPTS, 90 %) were purchased from Gelest (Morrisville, PA). Chloroform was purchased from EMC (Billerica, MA). Bromine was purchased from Fisher Scientific (Pittsburgh, PA). Chloroform was purchased from EMD (Billerica, MA).

*Synthesis of Phosphonated MSNs*: The synthesis of MCM-41 was based on well-established published procedures. Cetyltrimethylammonium bromide (CTAB, 250 mg, 0.7 mmol) was dissolved in $H_2O$ (120 mL) and NaOH (875 μL, 2 M). The mixture was heated to 80 °C and kept stable for 30 minutes, followed by adding a mixture of tetraethyl orthosilicate (TEOS, 1.2 mL) and diethylphosphatoethyltriethoxysilane (DEPETS) (0.2 mL) drop-wise into the solution while stirring vigorously. The solution was kept at 80 °C for 2 h and as-synthesized nanoparticles were centrifuged and washed thoroughly with methanol.

*Disulfide Snap-top Attachment on Phosphonated MSNs*: MCM-41 (100 mg) was dispersed into dry toluene (10 mL), mixed with (3-mercaptopropyl) trimethoxysilane (24 μL, 0.1mmol), and refluxed for 12 h under nitrogen atmosphere. Thiol group modified MCM-41 (100 mg) was washed and dispersed again in anhydrous toluene (10 mL) in a second step. To prepare thiocyanogen, lead thiocyanate (800 mg) was dispersed in 10 mL chloroform and titrated by

bromine (200 μL) in chloroform (10 mL). The titration product mixture was filtered and the filtrate containing thiocyanogen in chloroform was light yellowish. 1-adamantanethiol (17 mg, 0.1 mmole) and as-synthesized thiocyanogen were added into the MSN toluene suspension. The disulfide oxidation reaction took four days under 4 ℃ and nitrogen gas atmosphere. As-synthesized material was yellowish and washed thoroughly with toluene, methanol and water.

*Loading of MXF and Drug Release Test by Continuously Monitored Fluorescence Spectroscopy*: MCM-41 (10 mg) with disulfide snap-tops was suspended in 1 mL of 40 mM MXF in PBS solution and rotated overnight. β-cyclodextrin (40 mg) was added into the solution as capping agent to prevent the drug from leaking out. After mixing the solution for another 12 h, the particles were centrifuged and washed thoroughly 4 times. MXF loaded MCM-41 with disulfide snap-tops (MSN-SS-MXF) was dried under vacuum overnight. Release of MXF from MSN-SS-MXF in solution was measured by fluorescence spectroscopy using a 5 mW 377 nm laser beam to excite MXF in solution within a glass vial and a charge coupled device (CCD) connected to a computer to detect and collect emitted fluorescence. Specifically, the dried MSN-SS-MXF powder was put at a corner of the bottom of the glass vial containing 10 mL DI water. A stir bar was placed at another corner of the glass vial and gently stirred to facilitate the cargo diffusion without significantly disturbing the nanoparticles at the other corner of the vial (Figure S5). Baseline fluorescence spectra were collected for 1 h to establish that there was no MXF leakage, and then 2-mercaptoethanol (200 μL) or glutathione (1 mL of a 100 mM stock conentration to yield a final glutathione concentration of 10 mM) was added to the suspension. This resulted in a dramatic increase in fluorescence emission in the supernatant fluid, indicating release of MXF. A release profile was constructed by integration of MXF emission peak area from 480 nm to 520

nm. After collecting data for 17 h, by which time the MXF was released completely, the MXF concentration in the solution was calculated based on the UV-Vis spectrum and standard curve by Beer's law.

*Bacteria*: *Francisella tularensis* subsp. *holarctica* Live Vaccine Strain (LVS) was obtained from the Centers for Disease Control and Prevention (Atlanta, GA). For *in vitro* experiments, LVS was grown from frozen stock on GCII chocolate agar plates for 3 days prior to being used to infect macrophages. For *in vivo* experiments, pre-titered LVS frozen stock was used directly to infect mice and was serially diluted and plated on agar plates after infection to confirm bacterial CFU in the stock. For use in the bioassay, *F. tularensis* subsp. *novicida* strain Utah 112 (*F. novicida*) was grown at 37 °C with aeration in trypticase soy broth supplemented with 0.2% cysteine (TSBC).

*F. novicida Bioassay*: MXF was eluted from 1 mg/mL of MSN-SS-MXF under a) aqueous conditions by PBS; b) aqueous reducing conditions by PBS and 2-mercaptoethanol; and c) organic reducing conditions by DMSO and 2-mercaptoethanol; mixed by end-to-end rotation for 1 h at room temperature; and centrifuged at 10,000 g for 10 min. The supernates (1.5 μL) were added to *F. novicida* in 3 mL TSBC at a starting optical density (O.D.) at 540 nm of 0.05. *F. novicida* broth cultures were grown at 37 °C with shaking at 200 rpm for 6 h. At the end of the incubation, the O.D. of the bacterial broth cultures was measured. The amount of releasable MXF from the nanoparticles was determined by comparing the O.D. of the bacterial cultures treated with the supernates to the O.D. of the cultures treated with standard concentrations of MXF. The concentration of DMSO in the samples was less than 0.05%, a concentration that has

no effect on bacterial growth. Either glutathione or 2-mercaptoethanol can be used as a reducing agent in this assay. We used 2-mercaptoethanol because it is inexpensive, readily soluble in both DMSO and PBS, easily added from liquid working stock in reproducible fashion, commonly used in mammalian cell culture media, and has no impact on *F. novicida* bacterial growth at the concentrations used.

*Macrophages*: Human monocytic THP-1 cells (ATCC TIB 202) were maintained in RPMI-1640 (Lonza) with 10% fetal bovine serum (Cellgro), 2 mM GlutaMAX (Life Technology), penicillin (100 IU) and streptomycin (100 μg $mL^{-1}$). Prior to use, the THP-1 cells were suspended in culture medium without antibiotics and treated with 100 nM phorbol 12-myristate 13-acetate (PMA; Sigma) for 3 days to mature the cells into a macrophage-like cell type.

*Efficacy in Killing F. tularensis in Infected Macrophages*: PMA-differentiated THP-1 macrophages were infected with *F. tularensis* LVS at a multiplicity of infection ratio of 10 bacteria to 1 THP-1 cell for 90 min at 37 °C, 5% $CO_2$ – 95% air atmosphere. Infected monolayers were washed to remove extracellular bacteria. Fresh medium with or without MXF, MSN-SS-MXF, or supernates from DMSO or PBS extracts of the MSN-SS-MXF was added to the infected macrophage monolayer. The concentration of DMSO in the samples was less than 0.02%, a concentration that does not impact macrophage viability or bacterial growth. The cultures were incubated in the continued presence of the treatment for one day. *F. tularensis* LVS was harvested from untreated cultures at 30 min and 1 day post infection to determine bacterial growth without treatment and from infected cultures at 1 day to assess the effect of treatment. The bacteria were harvested by lysing the infected macrophages with 1% saponin in

PBS and the lysate was serially diluted and plated on GCII chocolate agar plates. Bacterial CFU on agar plates were counted after incubation at 37 °C, 5% $CO_2$ – 95% air atmosphere for 3 days.

*Efficacy in Killing F. tularensis in a Mouse Model of Pneumonic Tularemia*: Eight-week old, female, pathogen-free BALB/c mice purchased from Taconic were acclimated for one week. Mice were infected by the intranasal route with 4000 – 8,000 CFU of *F. tularensis* LVS, a dose equivalent to about 6-12 times the $LD_{50,}$ respectively. Two mice were euthanized 5 h after infection (day 0) to establish the number of bacteria in the lung at the start of the experiment. An additional 3 mice were euthanized one day later (day 1) to determine bacterial growth over that time period. Mice were then sham-treated (3 mice/group), treated with free MXF (3 mice/group for each dose) or treated with MSN-SS-MXF (4 mice/group for each dose) by tail vein injection every other day for a week (days 1, 3, and 5 for a total of 3 treatments). Mice were euthanized one day after the last treatment (day 6). Lungs, livers, and spleens from infected mice that were sham treated or treated with free MXF or MSN-SS-MXF were homogenized in PBS, pH 7.4. The organ homogenates were serially diluted and plated on GCII chocolate agar plates containing sulfamethoxazole (40 μg $mL^{-1}$), trimethoprim (8 μg $mL^{-1}$), and erythromycin (50 μg $mL^{-1}$) to prevent growth of contaminants. The agar plates were incubated at 37 °C for 4 days at which time the number of bacterial colonies on each plate was counted.

*Biodistribution of MSN-SS-MXF In Vivo*: *F. tularensis*-infected mice were either sham-treated (3 mice) or treated with MSN-SS-MXF once (3 mice) or 3 times over 5 days (3 mice) and euthanized 24 h later, at which time their organs were harvested, homogenized in PBS, digested with 0.1% $HNO_3$, and analyzed by ICP-OES (ICPE-9000, SHIMADZU, Japan).

*Median-effect Plots*: Relative efficacies of free MXF and MSN-SS-MXF were subjected to median effect analysis. The fraction of inhibition for samples treated with different amount of MXF was calculated using bacterial CFU in base-10 logarithm (log CFU) with the equation: Fraction of inhibition = 1 – (log CFU from sample treated with a known concentration of MXF or releasable MXF from MSN-SS-MXF / log CFU from untreated sample). A median-effect plot[38] for MXF or MSN-SS-MXF was generated using MXF or MXF equivalent (MSN) dose in base-10 logarithm as the X-axis and the fraction of surviving bacteria divided by the fraction of killed bacteria in base-10 logarithm as the Y-axis.

*Statistics*: Statistical analyses were performed using GraphPad Prism software (version 5.01) and R 3.2.[64] Means were compared across groups using one way analysis of variance (ANOVA) using the Bonferroni criteria to adjust p values for multiple comparisons. Comparisons of mean bacterial log CFU in the lung, liver and spleen between mice treated with MSN-SS-MXF or an equivalent amount of free MXF were based on a logit transform linear dose response model for the log CFU results for free drug, not assuming parallel dose response relationships. The adjusted mean for treatment with free drug was computed under this model, adjusted to the equivalent dose of MSN-SS-MXF, along with the corresponding p value for comparing the adjusted free drug mean to the MSN-SS-MXF mean. A P value of 0.05 or less was considered statistically significant.

*Study approval*: All experiments with mice were conducted within the guidelines and according to the protocol approved by the UCLA Institutional Animal Care and Use Committee.

## *Acknowledgments*

*B.-Y.L., Z.L., and D.L.C contributed equally to this work. This work was supported by Defense Threat Reduction Agency Grant HDTRA1-13-1-0046. We thank Saša Masleša-Galić and Susana Nava for excellent technical assistance, Jeff Gornbein for performing statistical analyses, and Bastian Ruehle for designing the Table of Contents illustration.*

## *Supporting Information*

*Supporting Information is available from the Wiley Online Library or from the author.*

## References


1. S. Saslaw; H. T. Eigelsbach; J. A. Prior; H. E. Wilson; S. Carhart, *Arch. Intern. Med.* **1961,** *107*, 702-714.
2. S. Harris, *Ann. N. Y. Acad. Sci.* **1992,** *666*, 21-52.
3. D. T. Dennis; T. V. Inglesby; D. A. Henderson; J. G. Bartlett; M. S. Ascher; E. Eitzen; A. D. Fine; A. M. Friedlander; J. Hauer; M. Layton; S. R. Lillibridge; J. E. McDade; M. T. Osterholm; T. O'Toole; G. Parker; T. M. Perl; P. K. Russell; K. Tonat, *JAMA* **2001,** *285* (21), 2763-73.
4. P. C. Oyston; A. Sjostedt; R. W. Titball, *Nat. Rev. Microbiol.* **2004,** *2* (12), 967-78.
5. N. A. Twenhafel; D. A. Alves; B. K. Purcell, *Vet Pathol* **2009,** *46* (4), 698-706.
6. H. Chen; L. Wang; J. Yeh; X. Wu; Z. Cao; Y. A. Wang; M. Zhang; L. Yang; H. Mao, *Biomaterials* **2010,** *31* (20), 5397-407.
7. J. E. Lee; N. Lee; H. Kim; J. Kim; S. H. Choi; J. H. Kim; T. Kim; I. C. Song; S. P. Park; W. K. Moon; T. Hyeon, *J Am Chem Soc* **2010,** *132* (2), 552-7.
8. Q. He; Z. Zhang; F. Gao; Y. Li; J. Shi, *Small* **2011,** *7* (2), 271-80.
9. F. Ungaro; I. d'Angelo; C. Coletta; R. d'Emmanuele di Villa Bianca; R. Sorrentino; B. Perfetto; M. A. Tufano; A. Miro; M. I. La Rotonda; F. Quaglia, *J Control Release* **2012,** *157* (1), 149-59.
10. H. Pinto-Alphandary; A. Andremont; P. Couvreur, *International journal of antimicrobial agents* **2000,** *13* (3), 155-68.
11. Z. Li; D. L. Clemens; B.-Y. Lee; B. J. Dillon; M. A. Horwitz; J. I. Zink, *ACS Nano* **2015,** *9* (11), 10778–10789.

12. A. A. Hwang; B. Y. Lee; D. L. Clemens; B. J. Dillon; J. I. Zink; M. A. Horwitz, *Small* **2015,** *11*, 5065- 5078.

13. D. L. Clemens; B. Y. Lee; M. Xue; C. R. Thomas; H. Meng; D. Ferris; A. E. Nel; J. I. Zink; M. A. Horwitz, *Antimicrob Agents Chemother* **2012,** *56* (5), 2535-45.

14. D. Tarn; C. E. Ashley; M. Xue; E. C. Carnes; J. I. Zink; C. J. Brinker, *Acc Chem Res* **2013,** *46*, 792–801.

15. C. Argyo; V. Weiss; C. Bräuchle; T. Bein, *Chemistry of Materials* **2014,** *26* (1), 435-451.

16. S.-H. Wu; C.-Y. Mou; H.-P. Lin, *Chemical Society Reviews* **2013,** *42* (9), 3862-3875.

17. Z. Li; J. C. Barnes; A. Bosoy; J. F. Stoddart; J. I. Zink, *Chem Soc Rev* **2012,** *41* (7), 2590-605.

18. C. Hwang; A. J. Sinskey; H. F. Lodish, *Science* **1992,** *257* (5076), 1496-502.

19. M. W. Ambrogio; T. A. Pecorelli; K. Patel; N. M. Khashab; A. Trabolsi; H. A. Khatib; Y. Y. Botros; J. I. Zink; J. F. Stoddart, *Org Lett* **2010,** *12* (15), 3304-7.

20. Y. M. Go; D. P. Jones, *Biochimica et biophysica acta* **2008,** *1780* (11), 1273-90.

21. F. Q. Schafer; G. R. Buettner, *Free radical biology & medicine* **2001,** *30* (11), 1191-212.

22. D. P. Jones; V. C. Mody, Jr.; J. L. Carlson; M. J. Lynn; P. Sternberg, Jr., *Free radical biology & medicine* **2002,** *33* (9), 1290-300.

23. D. P. Jones; J. L. Carlson; V. C. Mody; J. Cai; M. J. Lynn; P. Sternberg, *Free radical biology & medicine* **2000,** *28* (4), 625-35.

24. C. L. Anderson; S. S. Iyer; T. R. Ziegler; D. P. Jones, *American journal of physiology. Regulatory, integrative and comparative physiology* **2007,** *293* (3), R1069-75.

25. T. M. Guardado-Alvarez; L. S. Devi; J. M. Vabre; T. A. Pecorelli; B. J. Schwartz; J. O. Durand; O. Mongin; M. Blanchard-Desce; J. I. Zink, *Nanoscale* **2014,** *6* (9), 4652-8.

26. H. Kim; S. Kim; C. Park; H. Lee; H. J. Park; C. Kim, *Advanced materials* **2010,** *22* (38), 4280-3.

27. Q. Zhang; X. Wang; P.-Z. Li; K. T. Nguyen; X.-J. Wang; Z. Luo; H. Zhang; N. S. Tan; Y. Zhao, *Advanced Functional Materials* **2014,** *24* (17), 2450-2461.

28. Z. Luo; Y. Hu; K. Cai; X. Ding; Q. Zhang; M. Li; X. Ma; B. Zhang; Y. Zeng; P. Li; J. Li; J. Liu; Y. Zhao, *Biomaterials* **2014,** *35* (27), 7951-7962.

29. X. Ma; C. Teh; Q. Zhang; P. Borah; C. Choong; V. Korzh; Y. Zhao, *Antioxid Redox Signal* **2014,** *21* (5), 707-22.

30. P. Russell; S. M. Eley; M. J. Fulop; D. L. Bell; R. W. Titball, *J Antimicrob Chemother* **1998,** *41* (4), 461-5.

31. A. Chocarro; A. Gonzalez; I. Garcia, *Clin Infect Dis* **2000,** *31* (2), 623.

32. J. Steward; T. Piercy; M. S. Lever; A. J. Simpson; T. J. Brooks, *Int J Antimicrob Agents* **2006,** *27* (5), 439-43.

33. E. L. Nuermberger; T. Yoshimatsu; S. Tyagi; R. J. O'Brien; A. N. Vernon; R. E. Chaisson; W. R. Bishai; J. H. Grosset, *Am J Respir Crit Care Med* **2004,** *169* (3), 421-6.

34. S. Grayo; O. Join-Lambert; M. C. Desroches; A. Le Monnier, *Antimicrob Agents Chemother* **2008,** *52* (5), 1697-702.

35. H. Meng; M. Xue; T. Xia; Y. L. Zhao; F. Tamanoi; J. F. Stoddart; J. I. Zink; A. E. Nel, *J Am Chem Soc* **2010,** *132* (36), 12690-7.

36. A. Meister, *J Biol Chem* **1988,** *263* (33), 17205-8.

37. B. Morgan; D. Ezerina; T. N. Amoako; J. Riemer; M. Seedorf; T. P. Dick, *Nat Chem Biol* **2013,** *9* (2), 119-25.

38. T. C. Chou, *Pharmacol Rev* **2006,** *58* (3), 621-81.

39. Q. M. Jia; R. Bowen; J. Sahakian; B. J. Dillon; M. A. Horwitz, *Infect. Immun.* **2013,** *81* (5), 1550-1561.

40. Q. Jia; B. Y. Lee; D. L. Clemens; R. A. Bowen; M. A. Horwitz, *Vaccine* **2009,** *27* (8), 1216-29.

41. Q. Jia; B. Y. Lee; R. Bowen; B. J. Dillon; S. M. Som; M. A. Horwitz, *Infect. Immun.* **2010,** *78* (10), 4341-55.

42. S. Angelos; N. M. Khashab; Y. W. Yang; A. Trabolsi; H. A. Khatib; J. F. Stoddart; J. I. Zink, *J Am Chem Soc* **2009,** *131* (36), 12912-4.

43. K. Patel; S. Angelos; W. R. Dichtel; A. Coskun; Y. W. Yang; J. I. Zink; J. F. Stoddart, *J Am Chem Soc* **2008,** *130* (8), 2382-3.

44. S. Angelos; Y. W. Yang; K. Patel; J. F. Stoddart; J. I. Zink, *Angew Chem Int Ed Engl* **2008,** *47* (12), 2222-6.

45. M. W. Ambrogio; C. R. Thomas; Y. L. Zhao; J. I. Zink; J. F. Stoddart, *Acc Chem Res* **2011,** *44* (10), 903-13.

46. M. Xue; X. Zhong; Z. Shaposhnik; Y. Qu; F. Tamanoi; X. Duan; J. I. Zink, *J Am Chem Soc* **2011,** *133* (23), 8798-801.

47. M. Liong; S. Angelos; E. Choi; K. Patel; J. F. Stoddart; J. I. Zink, *Journal of Materials Chemistry* **2009,** *19* (35), 6251-6257.

48. M. Liong; J. Lu; M. Kovochich; T. Xia; S. G. Ruehm; A. E. Nel; F. Tamanoi; J. I. Zink, *ACS Nano* **2008,** *2* (5), 889-96.

49. V. Venketaraman; Y. K. Dayaram; A. G. Amin; R. Ngo; R. M. Green; M. T. Talaue; J. Mann; N. D. Connell, *Infect. Immun.* **2003,** *71* (4), 1864-71.

50. B. Arunachalam; U. T. Phan; H. J. Geuze; P. Cresswell, *Proc. Natl. Acad. Sci. U. S. A.* **2000,** *97* (2), 745-50.

51. A. Tamura; N. Yui, *Scientific reports* **2014,** *4*, 4356.

52. Q. Zhao; C. Wang; Y. Liu; J. Wang; Y. Gao; X. Zhang; T. Jiang; S. Wang, *Int J Pharm* **2014,** *477* (1-2), 613-22.

53. Q. Zhao; H. Geng; Y. Wang; Y. Gao; J. Huang; Y. Wang; J. Zhang; S. Wang, *ACS Appl Mater Interfaces* **2014,** *6* (22), 20290-9.

54. J. Zhang; M. Niemela; J. Westermarck; J. M. Rosenholm, *Dalton transactions* **2014,** *43* (10), 4115-26.

55. B. Zhang; Z. Luo; J. Liu; X. Ding; J. Li; K. Cai, *J Control Release* **2014,** *192*, 192-201.

56. Z. Yi; H. I. Hussain; C. Feng; D. Sun; F. She; J. E. Rookes; D. M. Cahill; L. Kong, *ACS Appl Mater Interfaces* **2015,** *7*, 9937−9946.

57. Y. Wang; N. Han; Q. Zhao; L. Bai; J. Li; T. Jiang; S. Wang, *European journal of pharmaceutical sciences : official journal of the European Federation for Pharmaceutical Sciences* **2015,** *72*, 12-20.

58. X. Wan; D. Wang; S. Liu, *Langmuir* **2010,** *26* (19), 15574-9.

59. J. T. Sun; J. G. Piao; L. H. Wang; M. Javed; C. Y. Hong; C. Y. Pan, *Macromolecular rapid communications* **2013,** *34* (17), 1387-94.

60. P. Nadrah; F. Porta; O. Planinsek; A. Kros; M. Gaberscek, *Physical chemistry chemical physics : PCCP* **2013,** *15* (26), 10740-8.

61. Z. Luo; K. Cai; Y. Hu; L. Zhao; P. Liu; L. Duan; W. Yang, *Angew Chem Int Ed Engl* **2011,** *50* (3), 640-3.

62. L. Dai; J. Li; B. Zhang; J. Liu; Z. Luo; K. Cai, *Langmuir* **2014,** *30* (26), 7867-77.

63. K. A. Hamblin; J. P. Wong; J. D. Blanchard; H. S. Atkins, *Front Cell Infect Microbiol* **2014,** *4*, 79.

64. R Core Team., *R Foundation for Statistical Computing, Vienna, Austria.* **2015,** *http://www.R-project.org/*.

## Supporting Information

# Redox-triggered Release of Moxifloxacin from Mesoporous Silica Nanoparticles Functionalized with Disulfide Snap-Tops Enhances Efficacy Against Pneumonic Tularemia in Mice

**Bai-Yu Lee, Zilu Li, Daniel L. Clemens, Barbara Jane Dillon, Angela A. Hwang, Jeffrey I. Zink, and Marcus A. Horwitz**

Dr. B.-Y. Lee, Prof. D. L. Clemens, B. J. Dillon, Prof. M. A. Horwitz
Division of Infectious Diseases
Department of Medicine
University of California
Los Angeles, CHS 37-121, 10833 Le Conte Ave., CA 90095-1688, USA
E-mail: mhorwitz@mednet.ucla.edu

Dr. Zilu Li, Dr. A. A. Hwang, Prof. J. I. Zink
Department of Chemistry and Biochemistry
University of California
Los Angeles, 3013 Young Dr. East
CA 90095-1569, USA
E-mail: jiz@chem.ucla.edu

Prof. J. I. Zink
California NanoSystems Institute
University of California
Los Angeles, CA 90095-8352, USA

Dr. Zilu Li
Department of Materials Science and Engineering
University of California
Los Angeles, CA 90095, USA

* B.-Y. Lee, Z. Li, and D. L. Clemens contributed equally.

Address correspondence to Marcus A. Horwitz, mhorwitz@mednet.ucla.edu or Jeffrey Zink, zink@ucla.edu

**Table S1**. Optimization of Uptake and Release Capacity

A. Influence of inner pore charges on MSNs uptake and release capacities

| Inner Pore Charges | Uptake Capacity (wt%) | Release Capacity (wt%) |
|---|---|---|
| Positive | ~ 0 | ~ 0 |
| Negative | 30.0 | 3.0 |

B. Influence of amount of phosphonate groups on MSN-SS uptake and release capacities

| Amount of DEPETS (μL) | Uptake Capacity (wt%) | Release Capacity (wt%) |
|---|---|---|
| 10 | 28.8 | 2.9 |
| 25 | 17.0 | 2.4 |
| 35 | 22.0 | 2.1 |

C. Influence of loading pH on MSN-SS uptake capacity

| Loading pH | Uptake Capacity (wt%) |
|---|---|
| 3 | 9.6 |
| 7.4 | 22.2 |

D. Influence of disulfide stalk surface coverage on MSN-SS uptake capacity

| Amount of Disulfide Stalk Surface Coverage (10 mg MSNs) | Uptake Capacity (wt%) |
|---|---|
| 10 μmol | 22.2 |
| 20 μmol | 19.7 |

E. Influence of MXF loading concentration on MSN-SS uptake and release capacities

| MXF Loading Concentration | Uptake Capacity (wt%) | Release Capacity (wt%) |
|---|---|---|
| 10 mM | 30 | 3 |
| 40 mM | 135 | 51 |

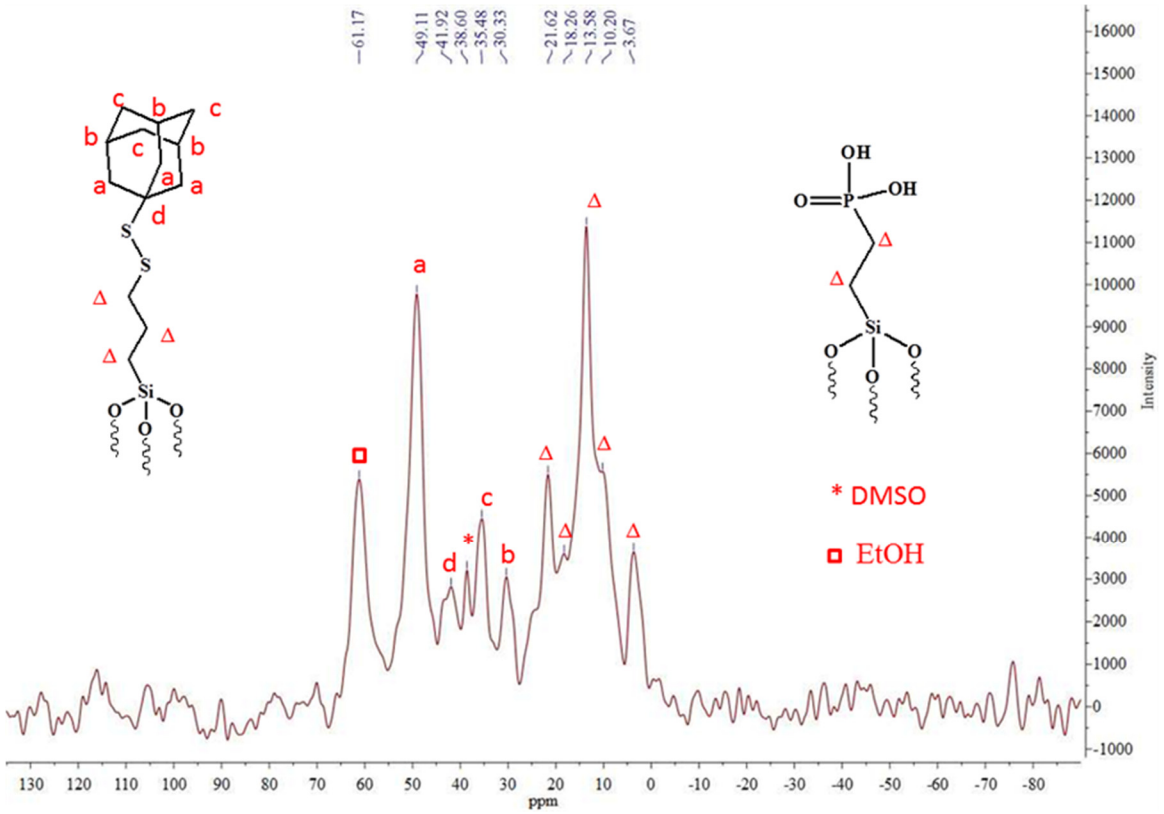


**Figure S1.** Adamantyl group attachment was confirmed by $^{13}$C-CPMS NMR spectroscopy

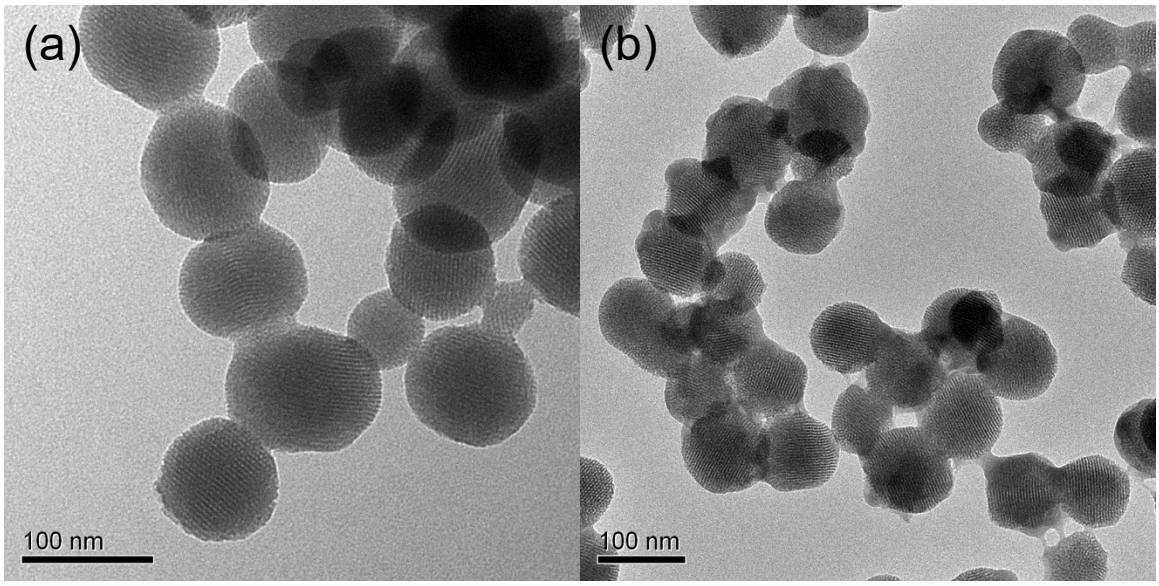


**Figure S2.** TEM images of MSN (a) before and (b) after surface modification with disulfide snap-top. The structural integrity preserved after all surface modifications and surfactant template extraction.

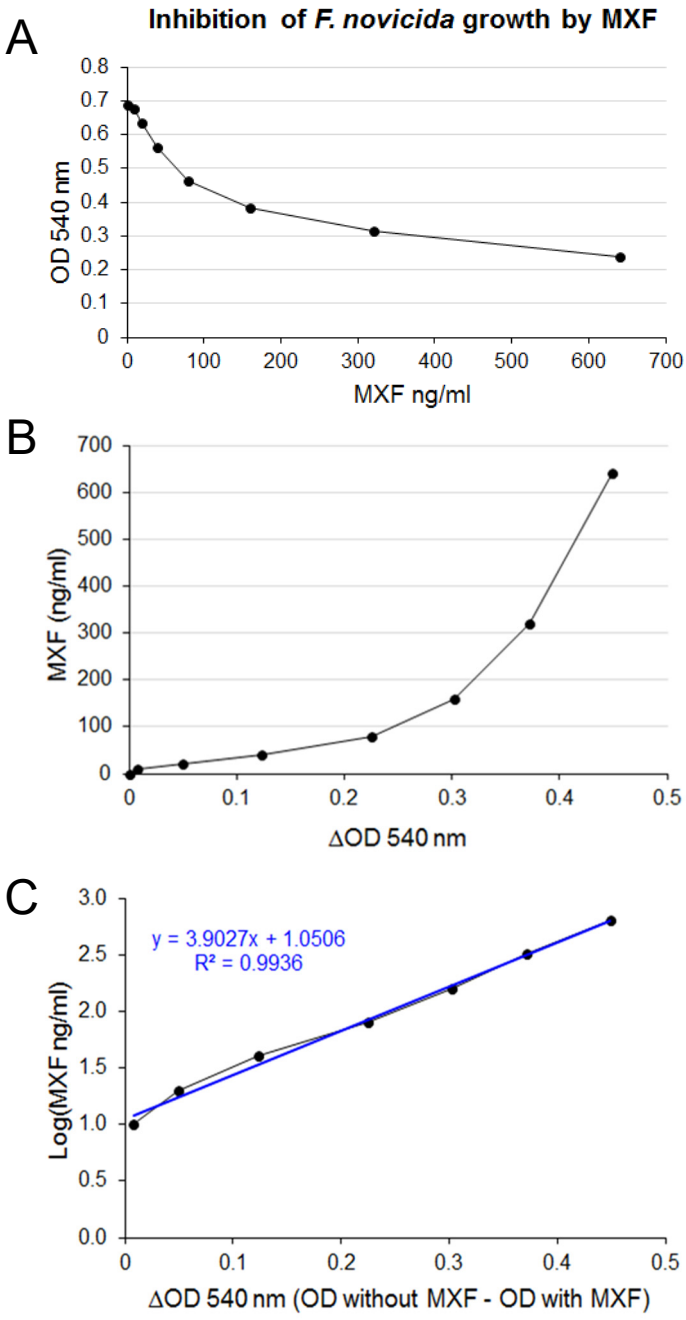


**Figure S3.** MXF loading on MSN-SS-MXF can be calculated from a MXF standard curve generated in the *F. novicida* bioassay. (A) Dose dependent inhibition of *F. novicida* growth by MXF at the concentrations indicated. (B) MXF concentrations plotted against the difference in $OD_{540}$ readings between an *F. novicida* culture not treated with MXF and a culture treated with MXF in the amounts indicated. (C) A linear standard curve converted from the log value of MXF concentrations plotted against the difference in $OD_{540}$ reading between an *F. novicida* culture not treated with MXF and an *F. novicida* culture treated with MXF.

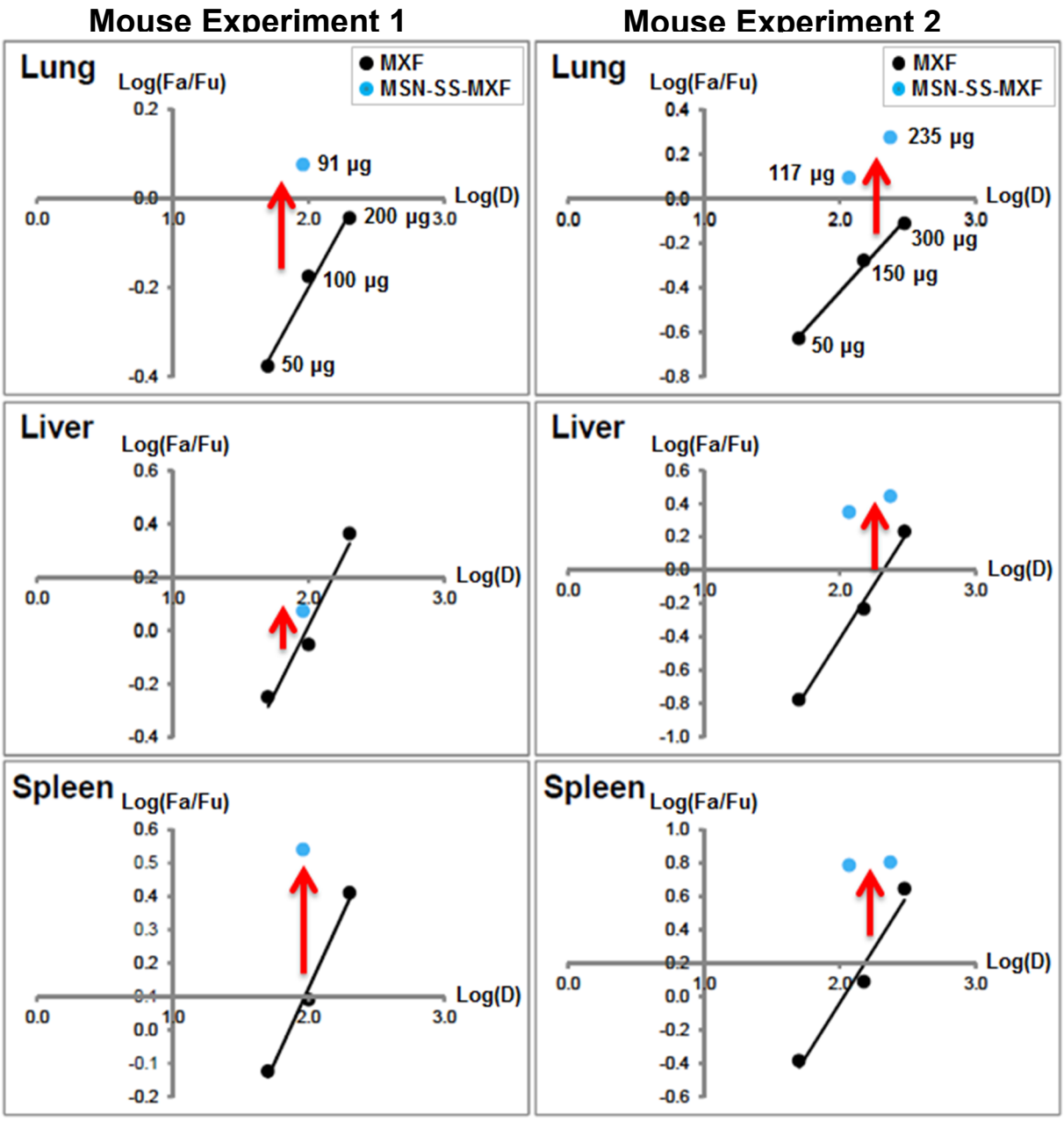


**Figure S4.** Median-effect plots to compare efficacy of MXF administered as free drug vs. MSN-SS-MXF. The efficacy of MSN-SS-MXF in the lung, spleen, and liver was compared to that of free MXF in a median-effect plot for mouse Experiments 1 and 2. For a given dose of MXF, an upward shift, as indicated by the red arrows paralleling the y-axis denotes a greater *F. tularensis* killing efficacy. Fa: Fraction of bacteria killed; Fu: Fraction of bacteria surviving; D: Dose of MXF in micrograms.

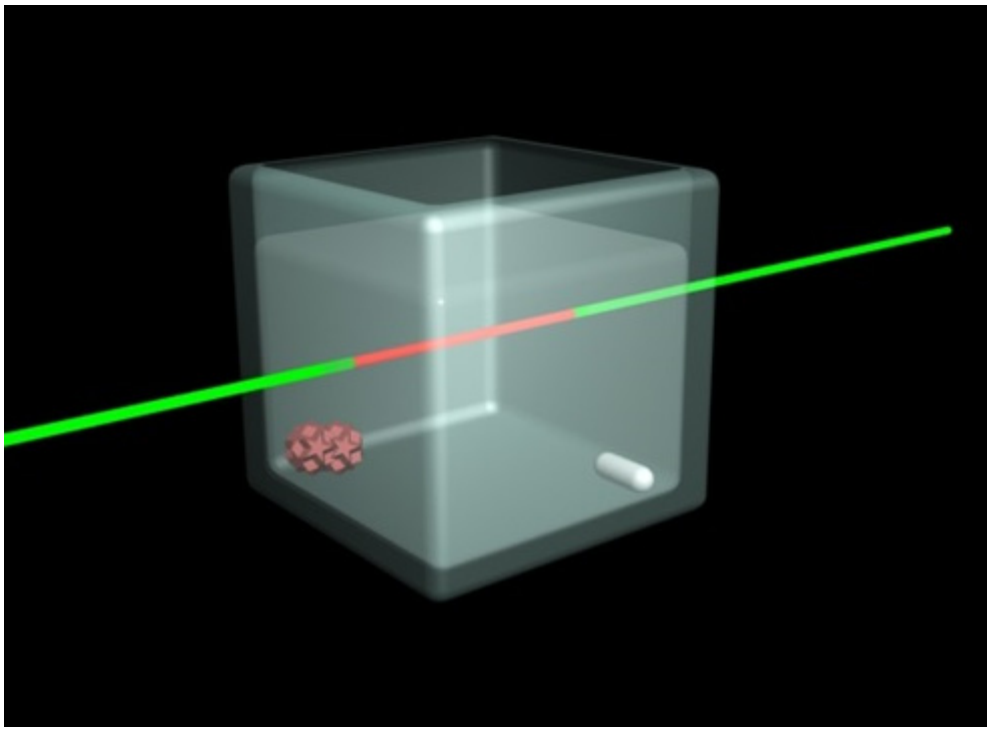

**Figure 5S. Drug release set up for continuously monitored fluorescence spectroscopy.**
Release of MXF from MSN-SS-MXF in solution was measured by fluorescence spectroscopy using a 5 mW 377 nm laser beam to excite MXF in solution within a glass vial and a charge coupled device (CCD) connected to a computer to detect and collect emitted fluorescence. MSN-SS-MXF was put at a corner of the bottom of the glass vial containing 10 mL DI water. A stir bar was placed at another corner of the glass vial and gently stirred to facilitate cargo diffusion without significantly disturbing the nanoparticles in the other corner of the vial.